Z-axis Contact Detection Algorithm for a Wire Bonder using a Discrete Kalman Filter

Jung-Han Kim[1, #]

1 School of Mechanical Design and Automation Engineering, Seoul National University of Technology, Seoul, South Korea
Corresponding Author / E-mail: hankim@snut.ac.kr; Tel: +82-2-970-6397; Fax: +82-2-974-8270

KEYWORDS : Detection algorithm, Stochastic parameters, Kalman filter, Filtering problem

We propose a new contact detection algorithm for fine pitch wire bonding. Fast and stable contact detection of the z-axis in wire bonding is extremely important to maintain the quality of fine pitch gold wire bonding processes, which use a small pad less than 70 μm in diameter. A small perturbation in the contact detection time causes a large difference in the size of the formed squashed ball. The new detection method is based on a statistical approach and designed for a discrete Kalman filter. It is faster and has smaller detection time variations than conventional detection methods. Experimental results are presented to demonstrate the advantages of the proposed algorithm..

Manuscript received: May 26, 2006 / Accepted: June 15, 2006

NOMENCLATURE

$\mathbf{b}_k$ = Input matrix
$\mathbf{F}_k$ = State transition matrix
$\mathbf{h}_k$ = Observation matrix
$\mathbf{P}_k$ = Error covariance matrix
$\mathbf{Q}_k$ = Covariance of process noise
$Q_k(k)$ = Contact test function
q_k = Chi-square test parameter
R_k = Covariance of measurement noise
v_k = Measurement noise
$\mathbf{v}_k$ = Innovation process
$\mathbf{x}_k$ = System state vector
$\mathbf{z}_k$ = Measurement value

1. Introduction

There is an increasing requirement for higher interconnection capabilities in semiconductor assembly processes. Recently, the number of interconnections in a typical semiconductor assembly process has increased remarkably, leading to smaller pads and balls in the wire bonding process.[1] Smaller pad sizes and finer pitches require new production control techniques, such as faster contact detection, precise force control, and smooth control mode changes in transient areas. These techniques have changed the structure of the wire bonder and necessitate a deeper understanding of the wire bonding process.

When the *z*-axis capillary contacts a pad, it impacts with a free air ball (FAB), and some part of the FAB forms an intermetallic boundary. After contact with the pad surface, the FAB is transformed into a squashed bonded ball by ultrasonic energy and the bonding force. Fig. 1 shows a magnified image of the pad side of the wire bonding process.

At the moment of contact, various factors affect the quality of the squashed ball, including the detection time, descent force, bonding force, and bonding temperature. Many parameters and factors influence the quality of the squashed ball; among these, the contact detection from noisy measurements plays a very important role in fine pitch wire bonding processes.[2] To obtain a uniform squashed ball size and consistent bonding quality, it is necessary to obtain accurate contact detection information for the *z*-axis, which is driven by a voice coil motor (VCM).[3]

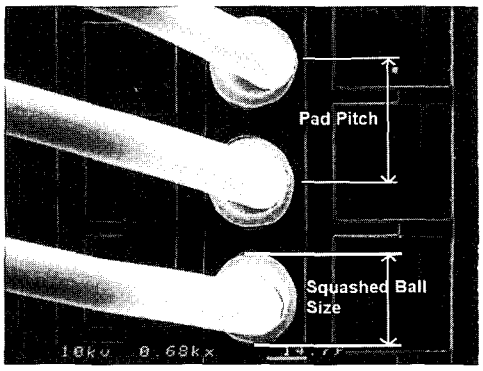

Fig. 1 Pad side in fine pitch gold wire bonding

The surface detection problem in wire bonding has common points with disturbance and failure detection problems in Kalman filter applications.[4] The detection of disturbances is closely related to model changes and parameter estimations, such as those found in a target tracking system. For example, with an airplane tracking problem, if a pilot accelerates or turns an airplane, the system model changes. In this case, the change in velocity must be identified from noisy measurements as soon as possible so that the system model in

the filtering algorithm can be updated. Blair[5] developed two-stage estimators and used the bias vector to detect changes in the system model. Failure detection using a generalized likelihood ratio test was also developed for multiple model changes. These related studies can be divided into three general categories: parameter estimation, parameter change detection, and multiple model changes. Researchers in the field of radar applications have been actively developing solutions to these types of problems for many years. For example, Bogler[6] used the residual of the Kalman filter to check its optimality. These problems share a common issue: how to detect model changes.

The present study is related to the detection of system changes. However, the detection methods found in target tracking systems are designed for tracking airplanes and are too complex to be installed in commercial control systems such as wire bonder machines. The present study presents very simple and effective test parameters that can be installed in conventional DSP motion control hardware. The new test parameters are designed for real-time contact detection of the z-axis of a wire bonder machine and can be easily calculated using the update parameters of a discrete Kalman filter. The following sections describe the design procedure of the new algorithm and the experimental results for a fine pitch wire bonding process.

2. Gold wire bonding process

2.1 Sequence of gold wire bonding

Gold wire bonding is characterized as a thermosonic process in which heat, ultrasonic energy, and force are used to execute the wire bonding. Fig. 2 shows the sequence of a typical gold wire bonding process. Two contacts occur during the formation of one wire. Generally, the first capillary contact is executed on the pad of the fabricated chip while the second contact is on the lead of the leadframe.

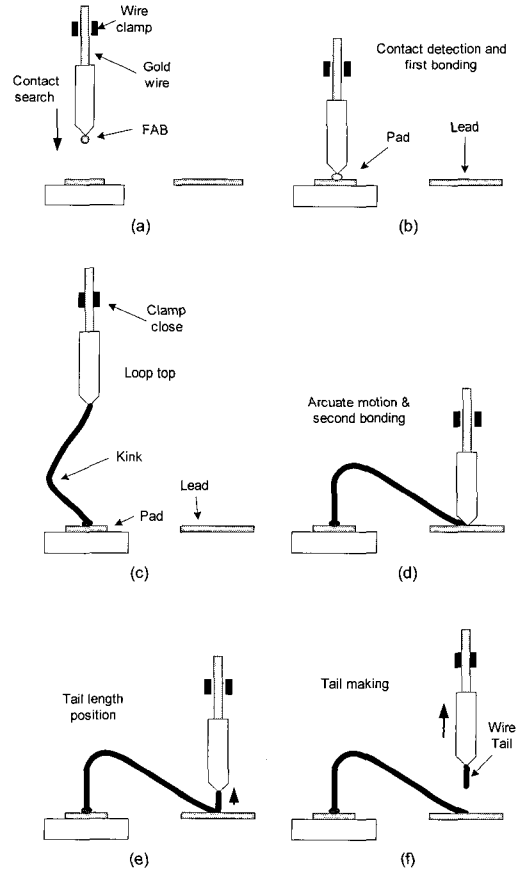

Fig. 2 Gold wire bonding sequence:
(a) capillary descends with gold ball,
(b) contact is made for the first bonding,
(c) a kink is formed and the process proceeds to the loop top,
(d) arcuate motion leads to the second bonding,
(e) the capillary proceeds to the tail length position, and
(f) the clamp is closed to form the tail

After the FAB formation, which uses an electronic flame-off (EFO) procedure, the capillary with a gold ball rapidly descends to the search level, and then proceeds to the pad surface with a constant speed until it contacts the pad (Fig. 2(a)). Every pad and lead has a slightly different contact level because variations always occur in the epoxy thickness and mechanical clamping status. After the first contact detection, the capillary is forced down by a bonding force with ultrasonic energy (Fig. 2(b)). When the first bonding process is complete, the capillary moves to the loop top position through a kink motion (Fig. 2(c)). It subsequently travels to the second search position with arcuate motion to find the second contact, at which time the second bonding occurs (Fig. 2(d)). After the second bonding, the capillary travels to the tail height with an opened wire clamp (Fig. 2(e)) and then moves to the EFO level with a closed wire clamp (Fig. 2(f)).

2.2 Disturbances for contact detection

There are three critical disturbances related to contact detection in the wire bonding process described above. The first disturbance is the electric current limitation of the z-axis to prevent damage to the chips during the capillary contact. Fig. 3 illustrates a capillary descending for contact. During the search for contact, the maximum control current of the z-axis must be limited to less than the bonding force, which has a typical value of 5 to 20 g for a pad. If the current of the z-axis is unlimited, the z-axis will push down the FAB at the moment of contact with a large control current until the contact is recognized, producing a large oversized squashed bonded ball. The limited current makes it difficult to control the z-axis with a constant velocity because the limited value is too small in the presence of disturbances from the spring hinge, cable tension, friction, and vibrations.

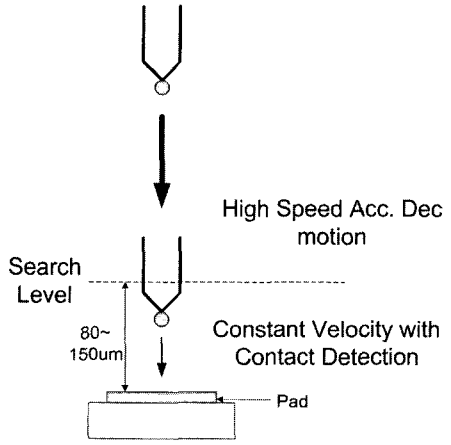

Fig. 3 Capillary descending before contact detection

The contact detection algorithms for the wire bonder are largely based on the z-axis velocity information. During the contact searching mode, the z-axis moves downward in a constant velocity control mode. At that time, if a certain disturbance causes an excessive velocity perturbation before contact, the detection algorithm will identify a false detection in the empty space, and consequently the control mode of the z-axis will be changed to the force control mode before an actual contact occurs. After that, the z-axis will impact and crush the silicon pad. For fine pitch wire bonding, the bonding force must be reduced substantially so that the velocity information and stable contact detection become critically important.

Another disturbance arises from mechanical structural vibrations. The z-axis descends with very high levels of acceleration and deceleration until it reaches the search level, which is generally 80 to

150 μm above the contact level. A state of the art wire bonder system has a maximum acceleration of 120 G for the z-axis, and consequently a large amount of excitation force for mechanical structural vibrations remains after deceleration. This vibration is a major obstacle to obtaining an accurate estimation of the z-axis velocity, and several IIR digital filters must be used to reduce the structural vibration noise in addition to the state estimator so that the contact detection algorithm is immune from the noise. Fig. 4 shows a front view of the wire bonding head, which has a long cantilever ultrasonic horn. The capillary is attached at the end of the ultrasonic horn.

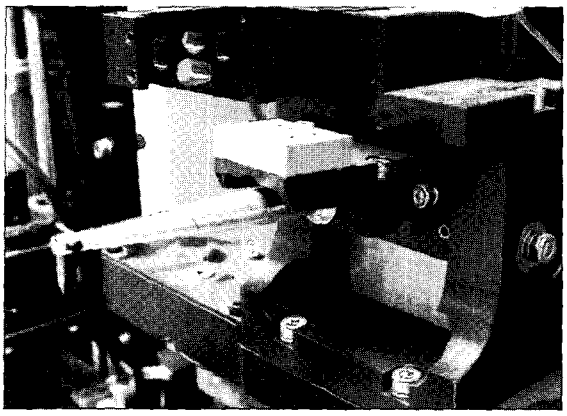

Fig. 4 Front view of the head of a wire bonder

A third disturbance for the contact detection problem arises from the gold wire feeding system. This system has several air blowers and a tensioner that cause wire vibrations during bonding. The gold wire vibration affects the z-axis velocity control during the contact search. The wire tensioner also affects the movement of the z-axis when the wire clamp is open. The thick line shown in Fig. 5 indicates raw velocity information obtained from simple differentiation of the encoder signal between control interrupts. Several IIR digital filters and a Kalman filter must be used to reduce this vibration noise.

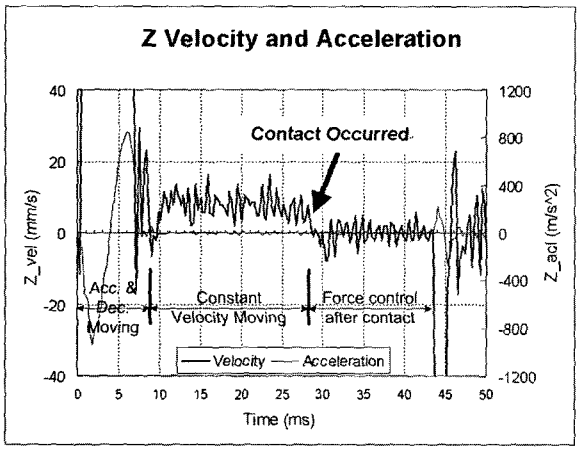

Fig. 5 Z-axis velocity and acceleration when the capillary contacts a pad

The aforementioned disturbances make it difficult to detect any contact with a stable detection time. This in turn affects the ball squash variation, which must be tightly controlled, especially for fine pitch wire bonding. The remaining sections of this paper describe the design of the velocity estimator and the contact detection algorithm.

3. Design procedure for the z-axis Kalman filter

For fine pitch wire bonding, the search velocity must be slower than that employed for a normal size pad because the impact force of the z-axis must be reduced. Therefore, the number of encoder pulses per control interrupt must be decreased. In this case, the velocity estimator becomes more important because the velocity information is used for one of the inputs of the contact detection algorithm. A z-axis moving with constant velocity can be modeled by the following equations:

$$\mathbf{x}_{k+1} = \mathbf{F}_k \mathbf{x}_k + \mathbf{b}_k u_k + \mathbf{G}_k \mathbf{w}_k, \tag{1}$$

$$z_k = \mathbf{h}_k \mathbf{x}_k + v_k, \tag{2}$$

$$\mathbf{x}_k = \begin{bmatrix} x_p \\ x_v \end{bmatrix}, \quad \mathbf{F}_x = \begin{bmatrix} 1 & \Delta t \\ 0 & 1 \end{bmatrix}, \quad \mathbf{h}_k^T = \begin{bmatrix} 1 \\ 0 \end{bmatrix}, \quad \mathbf{b}_k = \begin{bmatrix} \frac{1}{2}\Delta t^2 \\ \Delta t \end{bmatrix},$$

$$\mathbf{G}_k = \begin{bmatrix} 1 & 0 \\ 0 & 1 \end{bmatrix}, \tag{3}$$

where Δt is the sampling time, $\mathbf{G}_k$ is the process noise input matrix, and u_k is the acceleration input for the z-axis. The observation z_k is corrupted by the noise v_k, which has a variance of R_k. An electrical subdividing circuit is required to obtain finer resolution from an industrial encoder, which normally has a 4–20-μm grating pitch resolution. The phase subdividing circuit is composed of several analog components and A/D converters, and as such, the output of the subdividing circuit contains perturbations that largely come from electrical noise due to several sources, including thermal noise, shot noise, and burst noise. These intrinsic noises can be modeled as Gaussian distributions with a variance of R_k. The process noise $\mathbf{w}_k$ is also assumed to be Gaussian. The discrete Kalman filter equations can be written as

Time update:

$$\hat{\mathbf{x}}_{k/k-1} = \mathbf{F}_{k-1} \hat{\mathbf{x}}_{k-1/k-1} + \mathbf{b}_k u_k, \tag{4}$$

$$\mathbf{P}_{k/k-1} = \mathbf{F}_{k-1} \mathbf{P}_{k-1/k-1} \mathbf{F}_{k-1}^T + \mathbf{G}_{k-1} Q_{k-1} \mathbf{G}_{k-1}^T. \tag{5}$$

Measurement update:

$$\mathbf{K}_k = \mathbf{P}_{k/k-1} \mathbf{h}_k^T (\mathbf{h}_k \mathbf{P}_{k/k-1} \mathbf{h}_k^T + R_k)^{-1}, \tag{6}$$

$$\hat{\mathbf{x}}_{k/k} = \hat{\mathbf{x}}_{k/k-1} + \mathbf{K}_k (z_k - \mathbf{h}_k \hat{\mathbf{x}}_{k/k-1}), \tag{7}$$

$$\mathbf{P}_{k/k} = \mathbf{P}_{k/k-1} - \mathbf{P}_{k/k-1} \mathbf{h}_k^T (\mathbf{h}_k \mathbf{P}_{k/k-1} \mathbf{h}_k^T + R_k)^{-1} \mathbf{h}_k \mathbf{P}_{k/k-1}. \tag{8}$$

The key factor in designing an optimal estimator for Eqs. (4)–(8) is the determination of R_k and Q_k. The variance R_k can be determined by measuring the output of the subdivided encoder signal when the z-axis is tied to a stable block and the x–y stage is regulating the control status. A slow frequency drift can also be considered. The Q_k value has to be determined from actual bonding tests to account for all the disturbances described in Section 2. The velocity estimator may be used both in the searching area before contact and throughout the entire wire bonding process. If the estimated velocity information is used only in the contact searching area, the variance parameter R_k and Q_k can be specially optimized for the searching motion.

4. Design of the detection algorithm for the discrete Kalman filter

The bonding tip descends with constant velocity below the search level. Within this constant velocity region, the error covariance propagation (Eqs. (5) and (8)) oscillates, as illustrated in Fig. 6.[7] The difference between the two update processes (the second term of the RHS of Eq. (8)) indicates a reduction in uncertainty by reflecting the current measurement; therefore, if the measurement noise has a large covariance R, the amount of reduction will be small. When the bonding tip descends with constant speed, which is modeled with a

constant velocity model, the error covariance difference between the two update processes is statistically equal to the length of the vertical line drawn for each step in Fig. 6.

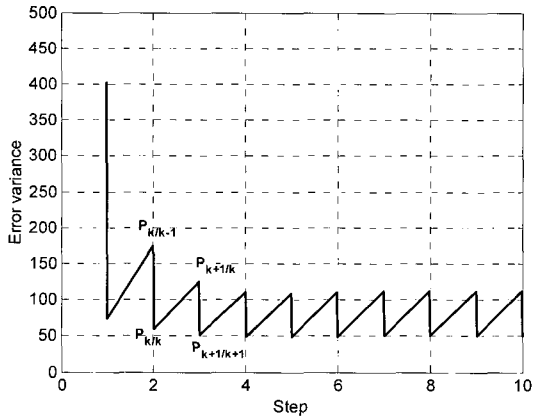

Fig. 6 Error covariance propagation of a Kalman filter

The difference between the two update processes (the vertical line drawn for each step) shows a reduction in the error covariance due to the measurements and filtering, and can be used as a reference to determine whether the velocity perturbations arise from noise or from actual contact. If the difference can be described as a certain parameter that includes actual measurements, it is possible to verify in real time whether the bonding tip achieves contact. In other words, the normalized vertical line of Fig. 6 can be used as a reference for the contact detection decision at each sampling moment. Theorem 1 connects the measure of expectation to the actual measurement space.

Theorem 1 The difference between the two covariance matrices can be described as an expectation function of an innovation process and optimal gain K,

$$\mathbf{P}_{k/k-1} - \mathbf{P}_{k/k} = E[\mathbf{K}_k \mathbf{v}_k \mathbf{v}_k^T \mathbf{K}_k^T], \tag{9}$$

where the innovation is $\mathbf{v}_k = \mathbf{z}_k - \mathbf{h}_k \hat{\mathbf{x}}_{k/k-1}$.

Proof. Given in the Appendix.

Theorem 1 describes the relation between the difference of the two covariance matrices and actual measurement data. The right side of Eq. (9) can be calculated from the innovation process, which includes the actual measurement data at each step. By using the left side of the predetermined statistical error covariance, it is possible to know whether the velocity of the bonding tip contacts the pad. For further development, a process c_i is defined as

$$c_i = \mathbf{h}_i \mathbf{K} \mathbf{v}_i. \tag{10}$$

It has a zero mean and a normal distribution because $\mathbf{v}_i$ is an innovation process.[8] Therefore, the square of c_i has a chi-square distribution. To verify the chi-square distribution in real time, Pearson's test statistic is introduced[9]:

$$q_k = \sum_{k-n}^{k} \frac{(c_i - E[c_i])^2}{\mathrm{var}(c_i)}, \tag{11}$$

where n denotes the size of the sample window. The variance of c_i is

$$E[(c_i - \bar{c}_i)(c_i - \bar{c}_i)^T] = E[c_i c_i^T] = E[\mathbf{h}_i \mathbf{K}_i \mathbf{v}_i \mathbf{v}_i^T \mathbf{K}_i^T \mathbf{h}_i^T]. \tag{12}$$

From Theorem 1, the variance of c_i can be represented by the difference between $\mathbf{P}_{i/i-1}$ and $\mathbf{P}_{i/i}$. If only the real measurable state is considered in the denominator of Eq. (11), the complete form of the equation using Theorem 1 is

$$q_k = \sum_{k-n}^{k} \frac{(c_i)^2}{\mathbf{h}_i(\mathbf{P}_{i/i-1} - \mathbf{P}_{i/i})\mathbf{h}_i^T} = \sum_{k-n}^{k} \frac{(\mathbf{h}_i \mathbf{K}_i \mathbf{v}_i \mathbf{v}_i^T \mathbf{K}_i^T \mathbf{h}_i^T)}{\mathbf{h}_i(\mathbf{P}_{i/i-1} - \mathbf{P}_{i/i})\mathbf{h}_i^T} \tag{13}$$

There is little additional computational cost to calculate the test parameter q_k because all the matrices used in Eq. (13) are also necessary to update the discrete Kalman filter. The chi-square degree of freedom $(n - 1)$ is determined from the sampling frequency and the endurable detection delay.

Physically, the test parameter q_k is a statistical information parameter concerned with the change in velocity that results from contact of the bonding tip. By using a normalized parameter for q_k, it is possible to introduce a standard chi-square table to determine the threshold of the alarm level and the probability of false alarms (PFA). For example, when the window size is 6 (with 5 degrees of freedom) and the sampling frequency is 4 kHz, the 95% confidence is obtained if the threshold is set at 11.070, resulting in a detection delay of approximately 1.5 ms. In this manner, the PFA of the test parameter q_k is determined for a certain level of risk. In an actual manufacturing process, 95% confidence is insufficient for wire bonding; therefore, in this paper, a contact test function $Q(k)$, composed of a series of Pearson's test parameters, is proposed. Consider a unit step function defined as

$$1(k) = \begin{cases} 1 & k \geq 0 \\ 0 & k < 0 \end{cases}. \tag{14}$$

In this study, the final contact test function $Q(k)$ is suggested as;

$$Q(k) = 1(q_k - \alpha_k) \times 1(q_{k-1} - \alpha_{k-1}) \times 1(q_{k-2} - \alpha_{k-2}) \times \ldots \times 1(q_{k-n} - \alpha_{k-n}) \tag{15}$$

where α_k is a certain threshold level from the standard chi-square table and n is the number of q_k values to be considered. For example, when three samples of q_k are used and the confidence parameter α_k is set to 2%, 2%, and 1% for the k, $k-1$, and $k-2$ steps, respectively, the final PFA is 4 ppm, which is a level equal to a 6 σ process. The test function $Q(k)$ can be easily extended to use more than three samples by increasing the parameter n when the sampling frequency is higher.

Table 1 PFA example

Confidence level α_k			Probability of a False Alarm (ppm)
k	$k-1$	$k-2$	
3 %	3 %	2 %	18
3 %	2 %	1 %	6
2 %	2 %	2 %	8
2 %	2 %	1 %	4

5. Experimental bonding results

Fig. 7 presents a block diagram of the experimental bonding system. The resolution of the encoder was 0.438 μm and the sampling frequency was 4 kHz. Three IIR notch filters were used to reduce the vibration noise, and the velocity signal was filtered using e Kalman filter. The z-axis velocity was maintained at a constant value in the contact searching region by a velocity controller. At each measurement step, the Kalman filter gave the parameters $\mathbf{K}_k$, $\mathbf{P}_{k/k}$, and $\mathbf{P}_{k/k-1}$ to calculate q_k, which was used to determine the test function

$Q(k)$. This was compared with the standard chi-square table to determine whether contact had occurred. The degrees of freedom of q_k was 5.

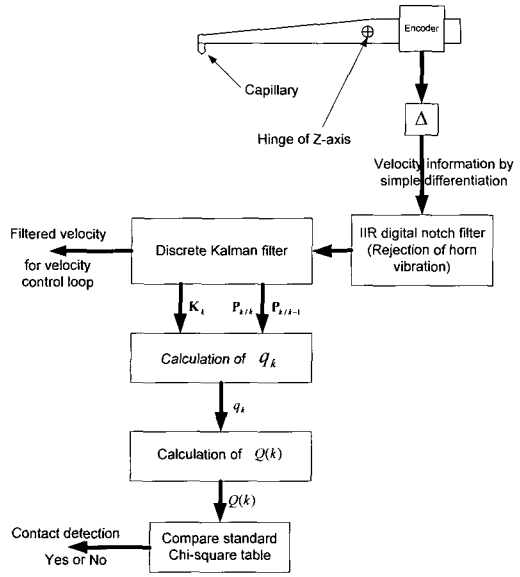

Fig. 7 Block diagram of the experimental system

As described in Section 2, the ultrasonic horn had a long structure, and hence the raw velocity information was corrupted with a large amount of vibration noise in the searching area, as illustrated in Fig. 5. Fig. 8 shows a bode plot of one of three IIR notch filters, which had a blocking frequency of 750 Hz, corresponding to one of the mechanical resonances. These digital filters introduced an additional phase delay in the control loop, causing more tracking errors. Therefore, the number of digital filters in the control loop should be minimized.

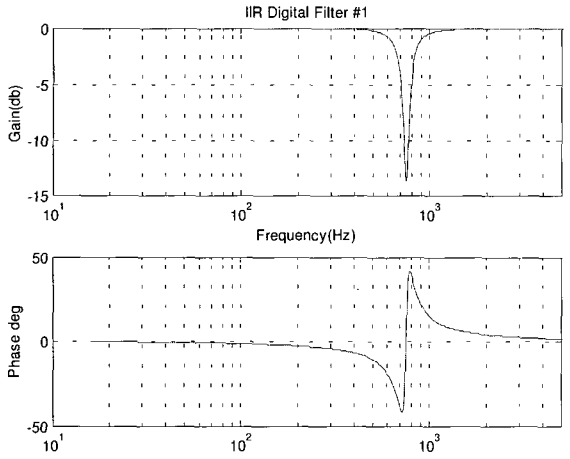

Fig. 8 Bode plot of a digital IIR notch filter used to reject vibration noise

Semiconductor devices with 126 or 208 pads and a 70-μm pad pitch were monitored in the tests. The experimental data were gathered in an actual wire bonding production line.

Fig. 9 shows the signal obtained when the capillary contacted a pad (window size n = 3, PFA = 8 ppm). In the tests, a four-channel D/A converter was attached to the DSP board that controlled the z-axis of the wire bonder. The parameters inside the DSP could be easily measured and captured in real time using the D/A converter. Fig. 9 shows four parameters inside the DSP that are related to the contact detection. Channel 1 gives the velocity output filtered with the Kalman filter described in Section 3. The trigger position was the moment that the z-axis passed through the search level, as illustrated in Fig. 2. Below the search level, the z-axis control mode was changed to a constant velocity mode for contact detection. Channel 2 shows the detection status flag obtained using the proposed method. This signal was maintained at approximately 1 V when it was ready to detect contact. Channel 3 shows the test parameter q_k, which is defined in Eq. (13). The detection decision value α_k for these tests was scaled at approximately 1.2 V with a 2% error for each q_k. Finally, channel 4, which was a test parameter used to check the algorithm, was a weighted summation of the q_k values.

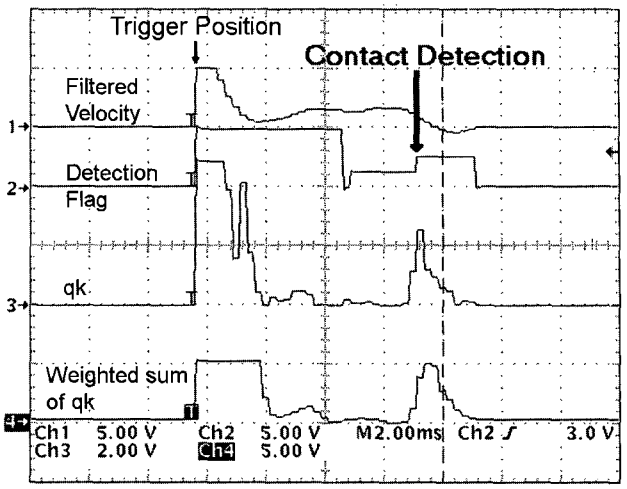

Fig. 9 Contact detection parameters:
Ch1: velocity information from the Kalman filter,
Ch2: detection status of the proposed algorithm,
Ch3: test parameter q_k, and
Ch4: weighted summation of the q_k values

The detection results of the test function q_k (channel 3) had a very fast response and produced a stable signal for actual wire bonding processes. The statistical design of $Q(k)$ provided systematic guidelines to manage the risk of false detection in a semiconductor assembly process, especially with regard to the mean time between assists (MTBA) in gold wire bonding.

To express the advantages of the proposed detection method numerically, the same test function given by Eq. (15), except for a constant threshold and filtered velocity instead of q_k, was compared with the results obtained using the proposed method. If the filtered velocity of the z-axis dropped below a certain threshold, the function outputted a contact detection flag in the first cell of Eq. (15).

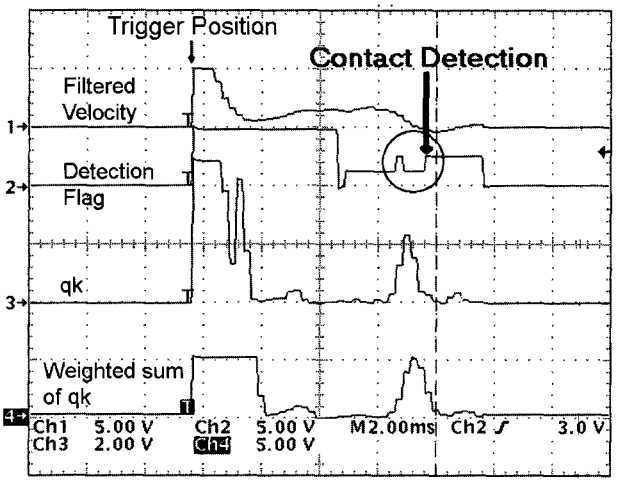

Fig. 10 Contact detection parameters:
Ch1: velocity information from the Kalman filter,
Ch2: detection status using a constant threshold,
Ch3: test parameter q_k, and
Ch4: weighted summation of the q_k values

In most cases, the velocity information is an important parameter for detection, and detection algorithms usually have the serial

structure given by Eq. (15) to improve their reliability. Many types of current wire bonding machines use similar detection methods. The tests demonstrated that a constant threshold occasionally results in delayed outputs. Fig. 10 shows the detection timing delay obtained using a constant threshold. Channel 2 of Fig. 10 shows the delay time. The contact detection flag returned to its ready-to-detect status for 0.7 ms after contact before the detection was finally recognized. Thus, a wrong detection was interpreted due to noise in the detection sequence (Eq. (15)). During this delay, the capillary tip descended further and exerted more force on the gold ball on the pad, resulting in a larger squashed ball. A constant threshold cannot efficiently reject the disturbance from a noisy velocity signal because of its structural limitations. Channel 3 of the proposed algorithm shown in Fig. 10 illustrates the stable detection characteristics of q_k. Thus, Fig. 10 clearly shows that the proposed detection method can reject this perturbation efficiently under the same test conditions.

Three 126-pad chips (378 wires) and two 208-pad chips (416 wires) were tested, and the detection times were measured for an actual production line. The detection times were recorded for both methods for every contact moment of 794 wires. The reference time line was the instant that the capillary tip passed through an area located 1×10^{-6} inches above the contact level. Table 2 provides a summary of the experimental results for each device.

Table 2 Experimental detection time

	Constant threshold		Proposed detection algorithm	
Device	126 pads	208 pads	126 pads	208 pads
Mean time $\bar{t}_d$	3.23 ms	3.32 ms	3.04 ms	3.07 ms
Standard deviation σ	0.1233	0.1344	0.0615	0.0781
Average	$\bar{t}_d$ = **3.28** ms, σ = **0.1289**		$\bar{t}_d$ = **3.06** ms, σ = **0.0698**	

The detection time shown in Table 2 is the time between the reference time line and the acknowledged moment of contact detection. The 208-pad device had a softer substrate, and hence more time was required to detect the surface in both algorithms. For both devices, the proposed algorithm detected contact faster and with more stable signal characteristics, which is necessary in fine pitch gold wire bonding. The low standard deviation indicated stable performance of the detection algorithm, which is very important for stabilizing the bonding strength and quality in the wire bonding process. The standard deviation of the proposed algorithm was nearly half that obtained using a constant threshold method. A larger standard deviation indicates that the detection delay shown in Fig. 10 occurs with much higher frequency.

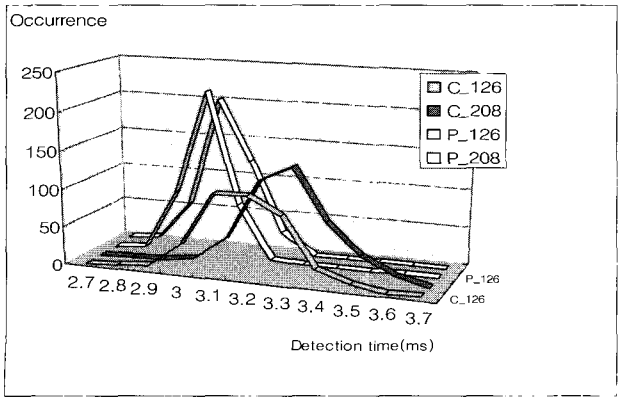

Fig. 11 Covariance plot of detection times

Fig. 11 graphically illustrates the mean and variation statistical characteristics for the detection time. The proposed method (P_126, and P_208) had a faster detection time with a narrower time variation.

6. Conclusions

In this paper, we proposed and tested a new contact detection algorithm for a wire bonder based on statistics. The contact detection time must be tightly controlled to facilitate finer pitch wire bonding. Variation of the detection time resulted in variations of the squashed ball size and unstable bonding quality. The proposed detection method was more stable and had faster detection times compared to the constant threshold detection method currently in use.

At each stage of the semiconductor manufacturing process, there is a certain range of variation in the characteristics of an individual device. Consequently, a statistical approach toward managing the output quality provides more stable quality in the final products from mass production processes. The statistical approach of the proposed algorithm is very useful when building stable processes in assembly production lines.

REFERENCES

1. Hwang, D. Y., Jeon, S. J. and Kim, K. B., "Development of the Flip-Chip Bonder using multi-DOF motion stage and vision system," Proc. of KSPE, pp. 1717-1722, 2003.
2. Leonhardt, D. A., "Fine pitch packaging: Trends and technology," Semicon West, 1997.
3. Kwon, K. H., Oh, S. H., Cho, N. G. and Yoon, J. Y., "Development of small loading and positioning device using VCM," Journal of KSPE, Vol. 20, No. 12, pp. 64-72, 2003.
4. Kwak, J. S. and Ha, M. K., "Detection technique of fault phenomena using power parameters in grinding process," International Journal of KSPE, Vol. 3, No. 1, pp. 5-12, 2002.
5. Blair, W. D., "Fixed-gain two stage estimators for tracking maneuvering targets," IEEE Transactions on Aerospace and Electronic Systems, Vol. 29, pp. 1004–1014, 1993.
6. Bogler, P. L., "Tracking a maneuvering target using input estimation," IEEE Transactions on Aerospace and Electronic Systems, AES-23, pp. 298-310, 1987.
7. Kim, J. H. and Oh, J. H., "A land vehicle tracking algorithm using stand-alone GPS," Control Engineering Practice, Vol. 8, pp. 1189-1196, 2000.
8. Kailath, T., "An innovation approach to least squares estimation part I: Linear filtering in additive white noise," IEEE Transactions on Automatic Control, AC-13, pp. 646-660, 1968.
9. Harvey, A. C., "Time Series Models," 2nd Edition, MIT Press, Cambridge, MA, pp. 41-45, 1992.

Appendix. Proof of Theorem 1.

Define

$$\tilde{\mathbf{x}}_{k/k} \equiv \hat{\mathbf{x}}_{k/k} - \mathbf{x}_k, \tag{16}$$

$$\tilde{\mathbf{x}}_{k/k-1} \equiv \hat{\mathbf{x}}_{k/k-1} - \mathbf{x}_k, \tag{17}$$

where $\mathbf{x}_k$ is the system state defined in Eq. (3). The innovation process is

$$\mathbf{v}_i = \mathbf{z}_i - \mathbf{h}_i \hat{\mathbf{x}}_{i/i-1}, \tag{18}$$

where v_k is the measurement noise term defined in Eq. (2).

$$E[(\hat{\mathbf{x}}_{k/k-1} - \hat{\mathbf{x}}_{k/k})(\hat{\mathbf{x}}_{k/k-1} - \hat{\mathbf{x}}_{k/k})^T] = E[(\tilde{\mathbf{x}}_{k/k-1} - \tilde{\mathbf{x}}_{k/k})(\tilde{\mathbf{x}}_{k/k-1} - \tilde{\mathbf{x}}_{k/k})^T]$$
$$= E[\tilde{\mathbf{x}}_{k/k-1}\tilde{\mathbf{x}}_{k/k-1}^T - \tilde{\mathbf{x}}_{k/k}\tilde{\mathbf{x}}_{k/k-1}^T - \tilde{\mathbf{x}}_{k/k-1}\tilde{\mathbf{x}}_{k/k}^T + \tilde{\mathbf{x}}_{k/k}\tilde{\mathbf{x}}_{k/k}^T] \tag{19}$$

Since

$$\tilde{\mathbf{x}}_{k/k} = \hat{\mathbf{x}}_{k/k} - \mathbf{x} = (\mathbf{I} - \mathbf{K}_k\mathbf{h}_k)\tilde{\mathbf{x}}_{k/k-1} + \mathbf{K}_k v_k \tag{20}$$

$$E[\tilde{\mathbf{x}}_{k/k-1}\tilde{\mathbf{x}}_{k/k-1}^T - \tilde{\mathbf{x}}_{k/k}\tilde{\mathbf{x}}_{k/k-1}^T - \tilde{\mathbf{x}}_{k/k-1}\tilde{\mathbf{x}}_{k/k}^T + \tilde{\mathbf{x}}_{k/k}\tilde{\mathbf{x}}_{k/k}^T]$$
$$= \mathbf{P}_{k/k-1} + \mathbf{P}_{k/k} - E[(\mathbf{I} - \mathbf{K}_k\mathbf{h}_k)\tilde{\mathbf{x}}_{k/k-1}\tilde{\mathbf{x}}_{k/k-1}^T + \mathbf{K}_k v_k \tilde{\mathbf{x}}_{k/k-1}^T$$
$$+ \tilde{\mathbf{x}}_{k/k-1}\tilde{\mathbf{x}}_{k/k-1}^T(\mathbf{I} - \mathbf{K}_k\mathbf{h}_k)^T + \tilde{\mathbf{x}}_{k/k-1}v_k\mathbf{K}_k^T]$$
$$= \mathbf{P}_{k/k-1} + \mathbf{P}_{k/k} - 2\mathbf{P}_{k/k} = \mathbf{P}_{k/k-1} - \mathbf{P}_{k/k}. \tag{21}$$

Equation (19) can be described in another form as

$$E[(\hat{\mathbf{x}}_{k/k-1} - \hat{\mathbf{x}}_{k/k})(\hat{\mathbf{x}}_{k/k-1} - \hat{\mathbf{x}}_{k/k})^T]$$
$$= E[\mathbf{K}_k(\mathbf{z}_k - \mathbf{h}_k\hat{\mathbf{x}}_{k/k-1})(\mathbf{z}_k - \mathbf{h}_k\hat{\mathbf{x}}_{k/k-1})^T\mathbf{K}_k^T], \tag{22}$$

Where

$$\hat{\mathbf{x}}_{k/k-1} - \hat{\mathbf{x}}_{k/k} = -\mathbf{K}_k(\mathbf{z}_k - \mathbf{h}_k\hat{\mathbf{x}}_{k/k-1}) = -\mathbf{K}_k\mathbf{v}_k$$
$$= E[\mathbf{K}_k\mathbf{v}_k\mathbf{v}_k^T\mathbf{K}_k^T]. \tag{23}$$